Environmental Science Processes & Impacts

ROYAL SOCIETY OF CHEMISTRY

PAPER

View Article Online
View Journal | View Issue

Cite this: *Environ. Sci.: Processes Impacts*, 2025, **27**, 1458

Physicochemical differences between wildfire pyrogenic carbon and slow-pyrolysis biochar suggest variations in elemental transport potential†

Katherine N. Snihur, *[a] Lingyi Tang,[a] Kelly J. Rozanitis, [a] Daniela Gutierrez-Rueda, [a] Cody N. Lazowski, [a] Daniels Kononovs,[a] Logan R. Swaren, ‡[a] Murray K. Gingras, [a] Janice P. L. Kenney, [bc] Shannon L. Flynn, [d] Kurt O. Konhauser [a] and Daniel S. Alessi [a]

Wildfires play a crucial role in the carbon cycle. Their contribution to the global carbon cycle is expected to increase with climate change as fire activity, particularly in boreal forests, escalates. As 8–28% of annually produced pyrogenic carbon is transported through riverine systems, its impact on fluvial environmental conditions will likely increase in coming years. However, the impact of pyrogenic carbon on metal and nutrient transport remains poorly understood. Here, we compare the chemical composition of wildfire-derived pyrogenic carbon (F-PyC) with slow-pyrolysis biochar-derived pyrogenic carbon (B-PyC), both originating from the same mountainous boreal forest biomass, to determine if F-PyC shares physicochemical properties with artificial B-PyC. The results reveal notable differences in the physicochemical properties and bulk composition of F-PyC compared to B-PyC, even when both are produced under similarly high temperatures, due to the rapid heating and cooling during wildfires. These differences in pyrolysis conditions result in F-PyC having a smaller ash fraction (<2.7% *vs.* >5.0%), a more acidic pH (<7.0 *vs.* >7.8), and a less thermally mature mineral composition and surface functionality. Together these differences in properties result in markedly different leaching behaviors and suggest that F-PyC and slow pyrolysis B-PyC play different roles in elemental transport. Consequently, this work supports earlier claims that B-PyC is not a suitable proxy for the F-PyC, particularly with respect to elemental transport in fluvial environments. Our work highlights the necessity for research specifically focusing on F-PyC to accurately quantify the contribution of wildfires to global elemental cycling, presently and in the geologic past.

Received 17th September 2024
Accepted 22nd April 2025

DOI: 10.1039/d4em00558a

rsc.li/espi

Environmental significance

This study is one of the first to quantify the physicochemical properties of wildfire derived pyrogenic carbon (F-PyC) and biochar (B-PyC) produced from the same feedstock and pyrolyzed at similar temperature ranges. We build on previous work to determine that the unique pyrolysis conditions that occur during a wildfire produces F-PyC that is physicochemically distinct from BPyC. These differences translate to markedly different leaching of inorganic elements inherent to the PyC when subjected to freshwater conditions, suggesting that studies that characterize the surface reactivity of B-PyC may not be applicable to interpretations of F-PyC reactivity in water. Our results highlight the need for geochemical research on F-PyC to understand its impacts on metals and nutrient cycling due to increasing global wildfire activity.

1. Introduction

Wildfire is a dominant carbon transformation process in natural landscapes, producing 2000 × 10^9 kg of $CO_{2(g)}$ and generating up to 385 × 10^9 kg of wildfire-derived pyrogenic carbon (hereafter referred to as F-PyC) each year.[1–5] Greenhouse gas emissions related to combustion are increasing regionally and predicted to continue to increase in many areas, including western North America, in response to climate change, with greater fire intensity and frequency.[6,7] This is particularly true in boreal and temperate forests, primarily due to increasing

[a]*Department of Earth and Atmospheric Sciences, University of Alberta, Edmonton, AB, T6G 2E3, Canada. E-mail: snihur@ualberta.ca*

[b]*Department of Physical Science, MacEwan University, Edmonton, AB, Canada*

[c]*School of Natural Sciences, Laurentian University, ON, Canada*

[d]*School of Natural and Environmental Sciences Newcastle University, Newcastle upon Tyne, UK*

† Electronic supplementary information (ESI) available: (1) Supporting methods including fire characteristics, tree identification, and supporting analysis methodology. (2) Supporting results and discussion as well as supplemental figures. (PDF). See DOI: https://doi.org/10.1039/d4em00558a

‡ Present addresses: Upstream Research, Imperial Oil Resources Limited, Calgary, Alberta, T2C 5R2, Canada.

growing season temperatures, changes to precipitation patterns, and increased extreme weather.[6,8–10] North American boreal forests, in particular, have been subject to an increase in wildfire activity, with more severe and frequent fires over the last several years, and a 111% increase in fire-prone conditions projected by 2100.[11,12] From 2020 to 2050, boreal forest fires in Canada and Alaska will generate an estimated 1330×10^{12} to $11\,930 \times 10^{12}$ kg CO_2, along with a significant but not estimated quantity of F-PyC.[11] Despite the prevalence of wildfires, the physicochemical properties of the F-PyC they produce and its role in metal and nutrient transport are not understood.

PyC broadly encompasses charcoal, black carbon, soot, and biochar, and, by definition, is a carbonaceous polycondensed aromatic product that is derived from the incomplete combustion of biomass, that is pyrolysis.[13–15] This material has the potential to sequester carbon for thousands of years at Earth surface conditions due to its resistance to biodegradation and weathering.[15] Chemically, PyC is made up of varying ratios of carbon (C), hydrogen (H), nitrogen (N), oxygen (O), and an inorganic ash fraction. Both the biomass composition and the pyrolysis conditions impact the relative composition. Biochar is a well-studied type of PyC, which we term B-PyC, and is generated under controlled temperatures and atmospheric composition *via* pyrolysis in controlled environments, such as furnaces.[16–21] It has been studied as a carbon sequestration strategy, an amendment to enhance soil fertility and crop growth, and as a remediation strategy to immobilize metals and organic contaminants in soil and water.[17,22–26]

In contrast to the tightly controlled conditions used for making B-PyC, the conditions during wildfires can vary in time and space. Wildfire temperatures often accelerate rapidly, with maximum temperatures often greater than 1200 °C.[27,28] It has been estimated that while these high temperatures are reached during wildfire, the pyrolysis temperatures are lower, capping at <1000 °C, with average temperatures around 700–750 °C.[26,28] These measurements, which taken by thermocouples indicate that the time at maximum temperature is short (*e.g.*, 176 s for temperatures >300 °C, suggesting that pyrolysis happens quickly in these environments.[28]

Following a wildfire, much of the F-PyC produced is transported to riverine environments and thus represents a substantial fraction of the organic carbon (C_{org}) transported through aqueous environments. For instance, in fluvial environments, F-PyC can comprise as much as $15.8 \pm 0.9\%$ of the total particulate organic carbon, an estimated 3.2×10^{10} per kg per C per year.[5] This equates to 8.3–27.6% of the F-PyC produced annually being transported *via* rivers and makes up a substantial portion of the PyC that is ultimately deposited into marine systems (0.48×10^{15}–1.44×10^{15} kg). While the fate of F-PyC upon reaching marine environments remains disputed, it has been speculated that is it deposited in marine sediments as a substantial C_{org} sink.[28,29] Not all F-PyC that is transported in riverine environments is deposited in marine sediments, as degradation of pyrogenic materials will occur as it moves through the F-PyC cycle. Despite the amount of F-PyC that moves through aqueous systems each year, its ability to transport elements and contribute to global elemental cycle is not well-constrained.

While F-PyC is recognized for its importance in carbon cycling and sequestration, its physicochemical properties remain understudied. This gap in research arises from the common assumption that B-PyC serves as a suitable proxy.[28,30–34] Considering the differing pyrolysis conditions, this leads to the unanswered question of whether F-PyC behaves similarly to B-PyC in its impacts on contaminant and nutrient transport. Addressing this question is critical for understanding the influence of wildfire on the global landscape, particularly that of other elemental cycles. In this study, we analyze the physicochemical properties, such as chemical composition and mobilizable fraction, of both F-PyC and B-PyC samples produced from similar feedstock biomasses collected from an area affected by a natural wildfire in British Columbia, Canada. Our goal is to discern how differences in pyrolysis conditions influence the physicochemical properties of the F-PyC and B-PyC derived from the same biomass. This understanding will provide new insights into the role of F-PyC in elemental cycling in natural environments, and ultimately determine if conventional B-PyC is a suitable proxy for F-PyC.

2. Methods

2.1 Fire characteristics and sample collection

Burned and unburned samples of pine (*Pinus* sp.), poplar (*Populus* sp.), and spruce (*Picea* sp.) were collected from within the fire perimeter of forest fire N42094 (BC Wildfire Service) near Golden, British Columbia, along the western slope of Mt. Hunter (Fig. S1†). The fire was active from July 20–October 23, 2021, and spanned 445 hectares (additional information on the fire characteristics is provided in ESI†). Samples were collected from October 2021–June 2022 from 7 locations and included 4 burned trees (three coniferous and one deciduous), and 3 unburned trees (two coniferous and one deciduous) (Fig. S2†). All 7 samples collected were exterior wood and bark, no deeper than 1 cm, as this depth represented the depth of charring on burnt samples. Burnt trees were selected to cover both deciduous and coniferous species having sufficient charring to collect representative samples. Samples were collected by scraping burned or unburned material from the trunk of the tree with a knife or hatchet, and the area was confined to approximately 30×30 cm^2. It is known that wildfire flame and pyrolysis temperatures fluctuate on a centimeter scale during a wildfire, so there may be some heterogeneity in the F-PyC samples collected.

2.2 Tree identification

Wood samples, collected from the inner wood of the tree in a 1–2 cm^3 sample, were thin-sectioned using a sliding microtome (AO Scientific Instruments, model #860), and stained using Safranin-O before identification using keys for thin-section identification of softwood and hardwood samples (Table 1).[35–38] Further information thin section preparation and species identification can be found in the ESI.† (ref. 36–41)

Table 1 Sample names and pyrolysis conditions of collected samples. All samples were a combination of bark and the outermost wood (<1 cm depth from the exterior of the tree)

Category	Sample ID	Species/Genus	Pyrolysis conditions
Source biomass	Sp(BM)	Spruce (*picea* sp.)	N/A
	Pi(BM)	Pine (*pinus* sp.)	N/A
	Po(BM)	Poplar (*populus* sp.)	N/A
B-PyC	Sp(300/6H/10)	Spruce (*picea* sp.)	300 °C for 6 hours with a heating rate of 10 °C min^{-1}, N_2 atmosphere
	Sp(700/6H/10)	Spruce (*picea* sp.)	700 °C for 6 hours with a heating rate of 10 °C min^{-1}, N_2 atmosphere
	Pi(700/6H/10)	Pine (*pinus* sp.)	700 °C for 6 hours with a heating rate of 10 °C min^{-1}, N_2 atmosphere
	Pi(700/5M/10)	Pine (*pinus* sp.)	700 °C for 5 minutes with a heating rate of 10 °C min^{-1}, N_2 atmosphere
	Pi(700/5M/30)	Pine (*pinus* sp.)	700 °C for 5 minutes with a heating rate of 30 °C min^{-1}, N_2 atmosphere
	Po(700/6H/10)	Poplar (*populus* sp.)	700 °C for 6 hours with a heating rate of 10 °C min^{-1}, N_2 atmosphere
F-PyC	F-PyC(Con)	Conifer (*picea* sp. or *pinus* sp.)	Wildfire, pyrolysis conditions unknown
	F-PyC(Po)	Poplar (*populus* sp.)	Wildfire, pyrolysis conditions unknown
	F-PyC(Pi-A)	Pine (*pinus* sp.)	Wildfire, pyrolysis conditions unknown
	F-PyC(Pi-B)	Pine (*pinus* sp.)	Wildfire, pyrolysis conditions unknown

2.3 Sample preparation

Unburnt wood samples were frozen at −25 °C upon collection to prevent decay. Before pyrolysis, samples were oven-dried at 60 °C for 5 days, to remove excess moisture. Samples were then crushed to a size of <1 cm and pyrolyzed at either 300 °C or 700 °C for 5 min or 6 hours (Across International STF1200 Tube Furnace), under anoxic conditions (with 400 cc min^{-1} N_2 gas) at a heating rate of 10 °C min^{-1} or 30 °C min^{-1} (Table 1). The feedstock was not agitated during pyrolysis and no quenching procedure was used in the cooling process, as the furnace was allowed to cool naturally. The reasons for the aforementioned pyrolysis conditions were two-fold: firstly the slow pyrolysis conditions are representative of that of conventional slow-pyrolysis B-PyC, and 300–700 °C covers the standard range of pyrolysis temperatures used for this type of B-PyC. Secondly, the average temperature recorded during a controlled burn of a similar biome was approximately 750 °C, thus we wanted B-PyC of similar maximum pyrolysis temperature conditions to that of average F-PyC.[26,28] Laboratory-generated B-PyC and the collected F-PyC were crushed with a ceramic mortar and pestle and passed through a 200-mesh sieve for subsequent analyses. Sample names and pyrolysis conditions are summarized in Table 1.

2.4 Sample characterization

2.4.1 Thermal gravimetric analysis with evolved gas analysis (TGA–EGA). For TGA–EGA analysis, approximately 16 mg ground sample was loaded into an aluminum crucible and analysed using a Netzsch STA 449 F3 Jupiter TGA with a QMS 403 Quadro Aeolos. During analysis, the sample was heated from 35 °C at a rate of 10 °C min^{-1} to 1000 °C in an atmosphere of 20% O_2 and 80% He. Mass scans were made of the evolved gases during analysis for each M/Z between 10 to 150 every 11 seconds during the analysis.

2.4.2 Elemental composition. Pyrolyzed and raw biomass samples were measured for total C, H, N, and S using a PerkinElmer 2400 series II CHNSO Analyzer with combustion and reduction temperatures of 975 °C and 500 °C, respectively. The ash fraction was determined by heating the F-PyC and B-PyC to 500 °C in a muffle tube furnace (STF1200), under ambient oxygen conditions for 8 to 23 h.[16,42] The O concentration was determined by subtraction of all C, H, N, S, and the ash fraction. The trace metals content was determined by aqua regia digestion of the ash fraction, following a protocol similar to von Gunten *et al.* (2017), and then corrected to a concentration in bulk F-PyC.[16] Briefly, 1 mL 70% ACS grade HNO_3 and 3 mL 37% ACS grade HCl were added to 0.05 to 0.1 g of solid sample and then allowed to react for 1 h at room temperature before heating at 80 °C for 1 h and 160 °C for an additional hour. Following the digestions, the solutions were cooled to room temperature and diluted to 50 mL with 18.2 MΩ ultrapure water. The samples were then filtered with 0.22 μm ashless filters (Cotton Linters) to remove undissolved particles, and elemental concentrations in the filtrates were measured with an Agilent 8800 inductively coupled plasma mass spectrometer (ICP-MS/MS). The silica content was determined from the residual solid fraction, by drying in the oven at 105 °C for 12 h followed by ashing in the muffle furnace at 750 °C for 30 min.[43] The sample pH was measured by mixing 0.5 g of ground unwashed sample in 50 mL of 18.2 MΩ·cm ultrapure water until the pH stabilized (24 h), after which the pH was measured.

2.4.3 Mobilizable fraction. The mobilizable fractions of the ground bulk B-PyC and F-PyC were determined through 5 sequential treatments using 0.01 M NaCl. Each treatment was done by adding 35 mL 0.01 M NaCl to 3.5 g of bulk, crushed F-PyC, and mixing the slurry for 3 hours on a rotator. The sample was then filtered through a 0.1 μm polyethersulfone (PES) membrane to remove the filtrate. The residual F-PyC was then resuspended in the same fashion 4 additional times to a total of 5 sequential treatments. By filtering and removing the solvent after each treatment, we were able to represent the periodic influx of freshwater in the environment. While the ratio of F-PyC to 0.01 M NaCl is unlikely to be similar to those found in the

natural environment, these treatments demonstrate elements which are available in the exchangeable fraction and would thus likely be removed from F-PyC given enough time. Additionally, these experiments are able to provide insight into the likely mineralogical composition through subsequent modelling. The speciation of the aqueous solutions was modeled using PHREEQC v. 3.5, and the saturation indices calculated to determine potential mineralogical controls on the leached elements.[44,45] The list of measured elements can be found in Table S3.† The phases were selected based on XRD data and elemental concentrations in the treatment samples. Further details on the methodology of the mobilizable fraction are provided in the ESI† section.

2.4.4 ICP-MS/MS. The elemental concentrations in experimental solutions generated by acid digestions or mobilization fraction treatments were measured using an ICP-MS/MS. In the case of digestions, where the total dissolved solids exceeded 2300 ppm, samples were diluted with 2% HNO3 and 0.5% HCl, a similar matrix to the aqua regia digestions. The mobilizable fraction samples were analyzed without further dilution and were acidified to pH < 2 using minimal acid to ensure concentrations remained above detection limit (12 μL of 70% HNO3 (ACS grade) per 10 mL of sample, amounting to 0.084%). A combination of no-gas and gas collision/reaction cell (He, O_2, or H_2) modes were used for the analysis. All measurements were taken using tandem MS/MS mode. Additional ICP-MS/MS parameters including element-specific information, standards, and internal standards used can be found in the ESI.†

2.4.5 TOC/TIC. The total organic carbon (TOC), total inorganic carbon (TIC), and water content of the B-PyC and F-PyC samples were determined using a multiphase carbon and water determinator (Leco RC-612). Approximately 15 mg of each sample was weighed and placed in a quartz (SiO_2) crucible. Samples were then heated in a pure oxygen atmosphere from 100 to 450 °C over 6 min, held at 450 °C for 65 seconds, and then heated to 450 to 1000 °C for 9 min. The CO_2 generated from 100 to 450 °C equates to the TOC, while the CO_2 generated from 100 to 1000 °C is assumed to be equivalent to the TC. TIC was calculated as the difference.

2.4.6 X-ray Diffraction. To constrain what mineralogical changes occur during washing, the mineralogical composition of samples both before and after the mobilization fraction experiments were measured by a Rigaku Ultima IV X-ray Diffraction (XRD) instrument using a Co tube radiation source and D/Tex Ultra detector. A continuous scan with an axis of 2Θ/Θ and range of 5–90° at a scan speed of 2.0° min^{-1} was used. The step size was 0.0200°. Data were converted using JADE MDI 9.6 software, and phase identification was done using DIFFRAC.EVA V5 software using the 2022/2023 ICDD PDF 4+ and PDF 4+/Organics databases.

2.4.7 Fourier transform infrared spectroscopy. Fourier transform infrared (FTIR) spectroscopy was used to determine bonding properties in the bulk material of all samples. To ensure that the proton conditions of the samples during FTIR analysis were consistent, all samples were suspended in 0.01 M NaCl to a concentration of 1 g L^{-1}, adjusted to pH 3, and then filtered through a 0.2 μm nylon membrane and dried before analysis. A pH of 3 was chosen to ensure functional groups were fully protonated and thus comparable between samples. Absorbance spectra were collected from 4000–400 cm^{-1} using a Bruker Tensor 27 FTIR spectrometer fitted with an A225/Q platinum ATR accessory with a diamond ATR crystal. Measurements were taken at a resolution of 4 cm^{-1} and 120 averaged scans were collected for background and sample measurements. The dried sample was pressed against the ATR crystal with a plunger during sample spectra collection. Final spectra were baseline corrected using an asymmetric least square fitting correction with a λ value of 300 000, a ρ of 0.001, and an area normalized over the spectral range of 900–1800 cm^{-1} using the script written by Felten *et al.*[46]

3. Results and discussion

3.1 Thermogravimetric analysis (TGA)

Derivative thermogravimetric analysis (DTG) and evolved gas mass spectra of BM (biomass), B-PyC, and F-PyC samples show the thermal degradation of remaining lignocellulosic structures, which can be applied to determine a range of maximum temperature of pyrolysis for materials.[47,48] Sp(BM) DTG curves show the three distinctive peaks of unpyrolyzed lignocellulosic materials, the dehydration of water at 73–83 °C, the cellulose degradation at 300–340 °C, and the degradation of lignin at 467 °C (Fig. 1A).[48] These peaks are accompanied by emissions spectra wherein DTG peaks at 73–83 °C coincide primarily with H_2O emissions (atomic masses of 17 and 18), while peaks at 300–350 °C coincide with emissions of H_2O, as well as CO and CO_2 (atomic mass 12 and 28, respectively), characteristic of cellulose thermal degradation. The high-temperature degradation peaks (467 °C) show evidence of the emission of carbon-containing gases (C, CO, and CO_2) which are characteristic of the non-carbohydrate, aromatic structure of lignin (Fig. S8†).[49] In the BM samples, all three peaks are present (Fig. 1 and S7A†).

Even with pyrolysis at 300 °C, as in Sp(300/6H/10), there is a complete loss of the hydration peak at 73–83 °C and a smoothing and shortening of the cellulose peak at 300–340 °C. Similarly, Sp(700/6H/10) shows a complete loss of both the dehydration and cellulose peaks, with only the lignin peak remaining. Unlike water and cellulose, lignin degrades over a large temperature range, 180–900 °C, thus the presence of the peak only confirms that the pyrolysis was <900 °C, or that pyrolysis was so rapid that lignin was unable to degrade fully.[48,49] The location of the lignin peak will move depending on the temperature of pyrolysis, such that a lignin peak at higher temperatures indicates that pyrolysis occurred at hotter temperatures.[47] This is observed in Fig. 1A, where the lignin peak of Sp(300/6H/10) is at a lower temperature than Sp(700/6H/10). The temperature dependence of these peaks is influenced by the biomass type of the B-PyC, with the Po(700/6H/10) reaching higher thermal stability, which is the temperature at which the compounds degrade, than the coniferous B-PyC samples pyrolyzed in the same way (Sp(700/6H/10 and Pi(700/6H/10); Fig. S7B†). However, does not appear to be influenced by the rate of pyrolysis of B-PyC, where no clear trend with accelerated pyrolysis is observed, as Pi(700/5M/10), reported

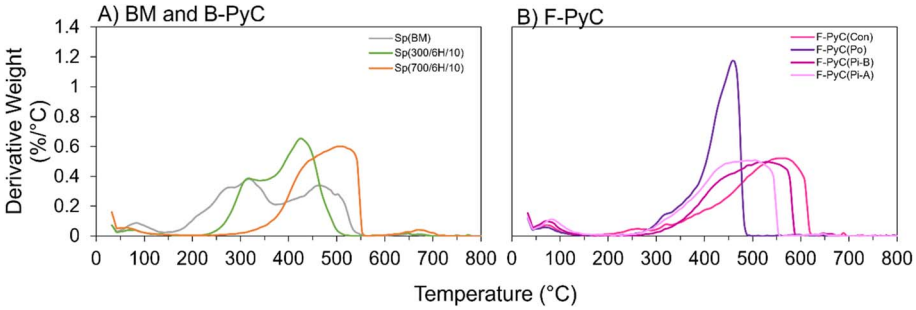

Fig. 1 DTG curves of (A) Spruce feedstock (Sp(BM), grey), and B-PyC (Sp(300/6H/10), 300 °C and Sp(700/6H/10), 700 °C) and (B) F-PyC samples (F-PyC(Con), F-PyC(Po), F-PyC(Pi-A), and F-PyC(Pi-B). No mass changes were observed at temperatures >800 °C, and thus these data were omitted.

a higher lignin peak than both Pi(700/6H/10) and Pi(700/5M/30). This indicates that within the limited ability of the muffle furnace to generate rapid pyrolysis, there is no trend with shortening the pyrolysis window (Fig. S7C†).

By using the B-PyC DTG and QMS spectra as a framework, it is possible to estimate the temperature of pyrolysis of the F-PyC samples. Due to the absence of a DTG peak at 300–340 °C and lack of emissions characteristic of the degradation of cellulosic carbohydrates at combustion temperatures in this temperature range, it is plausible that the F-PyC was pyrolyzed at temperatures greater than 340 °C (Fig. 1B and S8†). DTG of the F-PyC reveals that F-PyC(Con), F-PyC(Pi-A), and F-PyC(Pi-B) have high temperatures of mass stability, with degradation peaks for lignin from 513 °C to 573 °C, while F-PyC(Po) has a much lower temperature of lignin degradation at 462 °C (Fig. 1B). The temperature of the lignin peaks in F-PyC(Con), F-PyC(Pi-A), and F-PyC(Pi-B) are even higher than the B-PyC sourced from spruce at 700 °C, which has peaks consistent with the decomposition of lignin at 512 °C. This indicates that 3 of the 4 F-PyC samples were pyrolyzed at temperatures >700 °C. However, the presence of a lignin peak indicates the temperature of pyrolysis was <900 °C. This suggests that the maximum pyrolysis temperature was between 700–900 °C for F-PyC samples F-PyC(Con), F-PyC(Pi-A), and F-PyC(Pi-B), or the rapid wildfire pyrolysis of that seen in thermocouple data in previous work, was too fast to degrade the lignin and the maximum temperature of pyrolysis was higher.[28] Additionally, due to the lower temperature of the lignin peak for F-PyC(Po) when compared with Po(700/6H/10) (462 °C *vs.* 522 °C), F-PyC(Po) was likely pyrolyzed at temperatures between 350–700 °C. Alternatively, it is possible that some degradation of the structure of F-PyC(Po) occurred due to the delayed collection of this sample (8 months after the initial burn was reported). It is important to note that while TGA and DTG analyses of the B-PyC are well understood, very little study has been done TGA and DTG on F-PyC of known pyrolysis temperatures. It is possible that the process of combustion prior to pyrolysis during a wildfire, as well as varying amounts of oxygen during pyrolysis could impact the thermal stability of the resulting F-PyC. Generally the complete absence of peaks representing of hemi-cellulose and cellulose in F-PyC(Con), F-PyC(Pi-A), and F-PyC(Pi-B) indicate a higher pyrolysis temperature. Interestingly, the DTG curves of the F-PyC samples demonstrate a significant mass loss from 73–83 °C, representing water loss.[48] Neither Sp(300/6H/10) nor Sp(700/6H/10)) have this peak, suggesting water could be retained during rapid pyrolysis, or water was reintroduced through absorption following the wildfire event, and prior to sampling.[50] TGA analysis confirms that 3 of the 4 F-PyC were effectively pyrolyzed at temperatures between 700–900 °C or higher, similar to B-PyC samples produced at 700 °C. This allows us to make comparisons of other physicochemical properties of B-PyC and F-PyC produced from the same biomass. This determination is important to further understand and compare the implications of F-PyC and slow pyrolysis B-PyC in fluvial systems.

3.2 Pyrogenic carbon composition

The physiochemical properties of B-PyC samples, including major element (C, H, N, and O) composition, ash fraction, pH, water content, TIC, and TOC, follow trends related to the pyrolysis conditions that are similar to those observed in the literature (Fig. 2).[51–53] It is common to report C, H, and O data in a van Krevelen plot, which shows the degree of aromaticity (H/C) compared to the polarity (O/C), where the aromaticity increases with a decreasing atomic H/C ratio and polarity increases with an increasing atomic O/C ratio. With B-PyC, increasing pyrolysis temperatures result in a shift towards the origin of the plot, with the smallest H/C and O/C ratios reported for the highest pyrolysis temperature. The trend of increasing aromaticity and decreasing polarity as pyrolysis temperature increased was observed for the B-PyC samples with the 700 °C B-PyC samples, Sp(700/6H/10), Pi(700/6H/10), Po(700/6H/10), Pi(700/5M/10, and Pi(700/5M/30), falling the closest to the origin of the plot regardless of the source biomass (Fig. 2A). It should be noted that the shorter pyrolysis time of Pi(700/5M/10) and Pi(700/5M/30) results in reduced charring and therefore less dehydration and volatilization of oxygen and hydrogen, such that the samples plot at somewhat lower temperatures along this trend despite pyrolysis occurring at the same maximum temperature of 700 °C, as seen in Po(700/6H/10), Pi(700/6H/10), and Sp(700/6H/10).

It has been reported that an increasing pyrolysis temperature results in a higher pH and greater ash fraction, due to the formation of alkali minerals and the loss of hydrogen, nitrogen, and oxygen.[53–55] This trend is confirmed with B-PyC

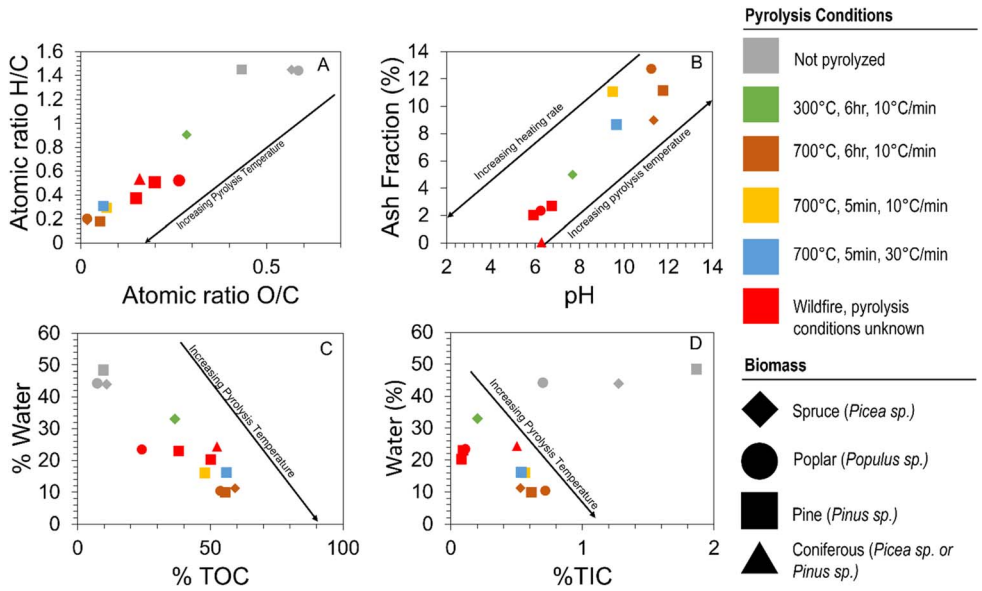

Fig. 2 Comparisons of physicochemical properties of biochar and F-PyC including (A) van Krevelen plot of elemental ratios, (B) the ash fraction compared with the pH, (C) water content compared with TOC, and (D) water content compared with TIC. Black arrows indicate pyrolysis parameter trends. Pyrolysis conditions, where known, are represented by a colour-coded system according to the legend, in the order of temperature, duration, and heating rate. The source biomass is represented by the shape of the data points.

samples with the highest ash fraction and pH reported in the high-temperature B-PyC samples (Sp(700/6H/10), Pi(700/6H/10), Po(700/6H/10), Pi(700/5M/10, and Pi(700/5M/30); Fig. 2B). Moreover, the pH of B-PyC has been shown to increase with higher maximum pyrolysis temperature due to a larger ash fraction containing Mg and Ca carbonate minerals (up to ~840 °C) and inorganic alkali metals, such as Na and K, up to ~890 °C and 760 °C, respectively.[53–55] Perhaps counter-intuitively, it has also been demonstrated that the pH and ash fraction decrease with increasing heating rate and/or decreased pyrolysis time. This is because alkali minerals, responsible for high pH and ash fractions require time at higher temperatures in order to form, which is not available during rapid pyrolysis.[51–53] This trend is also observed in the B-PyC samples when comparing the high-temperature Pine B-PyC samples, Pi(700/6H/10), Pi(700/5M/10, and Pi(700/5M/30). The reduced pyrolysis duration for both Pi(700/5M/10) and Pi(700/5M/30) resulted in a lower pH and ash fraction percentage than the Pi(700/6H/10), suggesting that the accelerated pyrolysis of Pi(700/5M/10) and Pi(700/5M/30) resulted in less inorganic minerals as in Pi(700/6H/10).

The water content of B-PyC decreases as the pyrolysis temperature increases (Fig. 2C and D). It is also well established that the TOC and TIC content increase with increasing pyrolysis temperatures, a trend that is observed in the B-PyC samples of this study.[53] The unpyrolyzed biomass samples have much higher water and TIC content and are not part of this trend. Of the high-temperature Pine B-PyC samples there was a higher water content in the fast pyrolysis samples, Pi(700/5M/10 and Pi(700/5M/30), compared to the slower pyrolysis sample, Pi(700/6H/10) (Fig. 2C and D). This suggests that the decreased residence time results in less water loss. This trend does not translate to the TOC or TIC, which are approximately the same regardless of pyrolysis rate. The absolute concentrations of the parameters shown in Fig. 1 can be found in Table S5.†

After determining that the maximum F-PyC pyrolysis temperatures were likely similar to those of the high temperature B-PyC (700 °C) through TGA analyses, direct comparisons were made with respect to other physicochemical properties. All four F-PyC samples, F-PyC(Con), F-PyC(Po), F-PyC(Pi-A), and F-PyC(Pi-B), plot on the van Krevelen diagram (Fig. 2A) between the B-PyC samples pyrolyzed at 300 °C (Sp(300/6H/10) and those pyrolyzed at 700 °C, such as Sp(700/6H/10), Pi(700/6H/10), Po(700/6H/10), Pi(700/5M/10, and Pi(700/5M/30)). This suggests that the charring intensity, which is a measure of the maximum pyrolysis temperature obtained and the duration at temperatures >200 °C, during pyrolysis was less than for the high-temperature B-PyC samples (700 °C).[28] This was due to the duration of pyrolysis which was likely shorter than for all B-PyC samples, including the rapid pyrolysis B-PyC samples, Pi(700/5M/10) (10 °C min^{-1}) and Pi(700/5M/30) (30 °C min^{-1}), which were both pyrolyzed for 5 min at a heating rate of 10 °C min^{-1} and 30 °C min^{-1}, respectively (Fig. 2A). This is further reinforced by the fact that all F-PyC samples plot in a similar location in the water content *vs.* TOC diagram (Fig. 2C), falling between B-PyC samples produced at 300 °C and 700 °C in both water content and TOC concentration, as the wildfire's rapid pyrolysis rates would limit the period of time for TOC conversion and water evaporation from the samples when compared with B-PyC pyrolysis durations. Interestingly, the pH and ash fraction of the F-PyC samples do not plot between the 300 °C and 700 °C B-PyC samples (Fig. 2B). All F-PyC samples are unique from B-PyC samples having an acidic pH (<7) and a lower ash fraction, 2.7% to <1%. This is even lower than the lowest temperature B-PyC, Sp(300/6H/10), at 5.0%,

further evidence of reduced charring intensity due to a shortened pyrolysis time.[51]

We interpret the low ash content and pH of the F-PyC as indicators of accelerated pyrolysis occurring during the wildfire. Rapid heating and a short time at the peak temperature have been observed during controlled forest fires where the observed T_{max} range was 550–976 °C and the duration of time at a temperature greater than 300 °C averaged less than 6 min.[28] Similarly, additional studies have found a range in maximum temperature of 400–1100 °C, with a flame time as short as 37 s.[56,57] Despite the large range in maximum temperatures, recorded wildfire temperature profiles suggest flash-like pyrolysis heating rates, with a short period at the maximum temperature.[27,28,30] By comparison, the fastest pyrolysis of this study was conducted with a heating time greater than 300 °C for 18 min (Pi(700/5M/30)), and with a longer cooling time. This suggests that the forest fire of this study burned and cooled more rapidly than the B-PyC pyrolysis conditions of this study, and rapid pyrolysis is likely the reason for the differences between the F-PyC and B-PyC data in Fig. 2B and D, and not differing maximum temperatures. It is also possible that fluctuating ambient oxygen levels following initial pyrolysis could impact the resulting F-PyC physiochemical composition. Despite an ongoing drought in the area, with no recorded precipitation in the area between the wildfire ignition and the collection of samples F-PyC(Con), F-PyC(Pi-A), and F-PyC(Pi-B), it is possible that wind and rain could have altered the physicochemical composition in the period of time between the wildfire and F-PyC sample collection. This is particularly true for that of F-PyC(Po) which was subject to an entire winter period of snow-cover and melt before collection.[58] These are both areas of research that require further study. The F-PyC pyrolysis conditions are thus substantially different from those of conventional B-PyC production. This suggests that while common trends in physicochemical properties, such as atomic ratios C/H and O/H, ash fraction, pH, water content, and TOC seen in B-PyC, may be applied to F-PyC, comparisons in the absolute values of the aforementioned physicochemical parameters between the two cannot.

The observed differences in aromaticity, polarity, pH and ash content would undoubtedly result in differing behaviours in fluvial environments. In particular, B-PyC is known to increase the pH of soil and water environments, and in fact it is often employed for that purpose.[59] With the acidic pH of F-PyC, the opposite effect would likely take place, where cations would adsorb weakly to the PyC, and anions more strongly. This would therefore impact water quality in a different way, as different elements would be transported. In addition, the smaller ash fraction of F-PyC indicated that lower elemental concentrations may leach into riverine waters. Therefore, studies using slow-pyrolysis B-PyC as a proxy to determine water quality in riverine systems following wildfire events would likely be incorrect.

The concentrations of inorganic elements varied based on the mineral fraction in each sample (Table S6†), but in general, the order of major elements from greatest to least abundant was: Ca → K → Mg → P → Si → S → Ba → Mn → Sr → Fe → Al → Na. To reconcile the variations in total measured concentrations, all concentrations were normalized as the percent of all measured inorganic elements. By plotting data in this way, it is possible to determine the changes in the mineral fraction of elements that resulted from differing pyrolysis conditions. For instance, by looking at the spruce biomass (BM) and B-PyC, it is possible to determine that increasing pyrolysis temperature, with a duration of 6 h, concentrates Ca and K while depleting Si (Fig. S9A†). In the same way, it is possible to determine the effect of pyrolysis duration and heating rate on the inorganic chemical composition by looking at Pi(BM) and B-PyC samples (Fig. S9B†). The same increase in Ca relative abundance is observed across both pine B-PyC samples that were pyrolyzed with a slow heating rate (Pi(700/6H/10) and Pi(700/5M/10). Interestingly, there is a lower relative abundance of Ca in Pi(700/5M/30) when compared to the other two pine B-PyC samples, Pi(700/6H/10) and Pi(700/5M/10), 55.94% *vs.* 58.95% and 67.90%, respectively, indicating that increased heating rates reduce the relative abundance of Ca. By the same note, there is an increase in relative Si abundance in the rapid pyrolysis sample, Pi(700/5M/30) (4.58%) when compared with the other two pine B-PyC samples (0.09% and 0.94% for Pi(700/6H/10) and Pi(700/5M/10), respectively). This suggests that rapid pyrolysis, which resulted in reduced charring intensity of F-PyC samples, caused reduced Ca and/or increased Si relative abundances when compared with high temperature B-PyC samples. Similar trends as those seen in spruce and pine pyrogenic materials are also seen in poplar BM, B-PyC, and F-PyC.

The inorganic elemental concentrations in the B-PyC were consistent with mineralogical analyses conducted using XRD (Table S7†). The greater Si concentration in Sp(300/6H/10) was attributed to the presence of quartz in that sample, which was not found in the other pyrolyzed samples. The high fraction of Ca correlated to the presence of Ca-bearing minerals, such as calcite ($CaCO_3$), portlandite ($Ca(OH)_2$), vaterite ($CaCO_3$), and whewellite ($CaC_2O_4 \cdot H_2O$), which were found in many of the samples (Table S7†). As the ash fraction was small (<3%) in the F-PyC samples, mineralogical analyses were unsuccessful.

3.3 Chemical characterization

FTIR spectroscopic analyses reveal the presence of distinct oxygen bonded molecules, which are the building blocks of most surface functional groups, in both F-PyC and B-PyC samples (Fig. 3). Samples were adjusted to pH 3 to ensure functional groups were similarly protonated, therefore observed changes were due to structural differences and not protonation/deprotonation reactions. The surface chemistry of B-PyC is dependent on the pyrolysis temperature.[33,60–62] Low temperature of pyrolysis of Sp(300/6H/10) preserves much of the original woody biomass, resulting in a complex spectrum with many peaks.[38] As temperature rose from 300 °C to 700 °C between Sp(300/6H/10) and Sp(700/6H/10), it resulted in four major changes between the spectra. First, there was a loss of many peaks, particularly in the 1550–1100 cm^{-1} region which

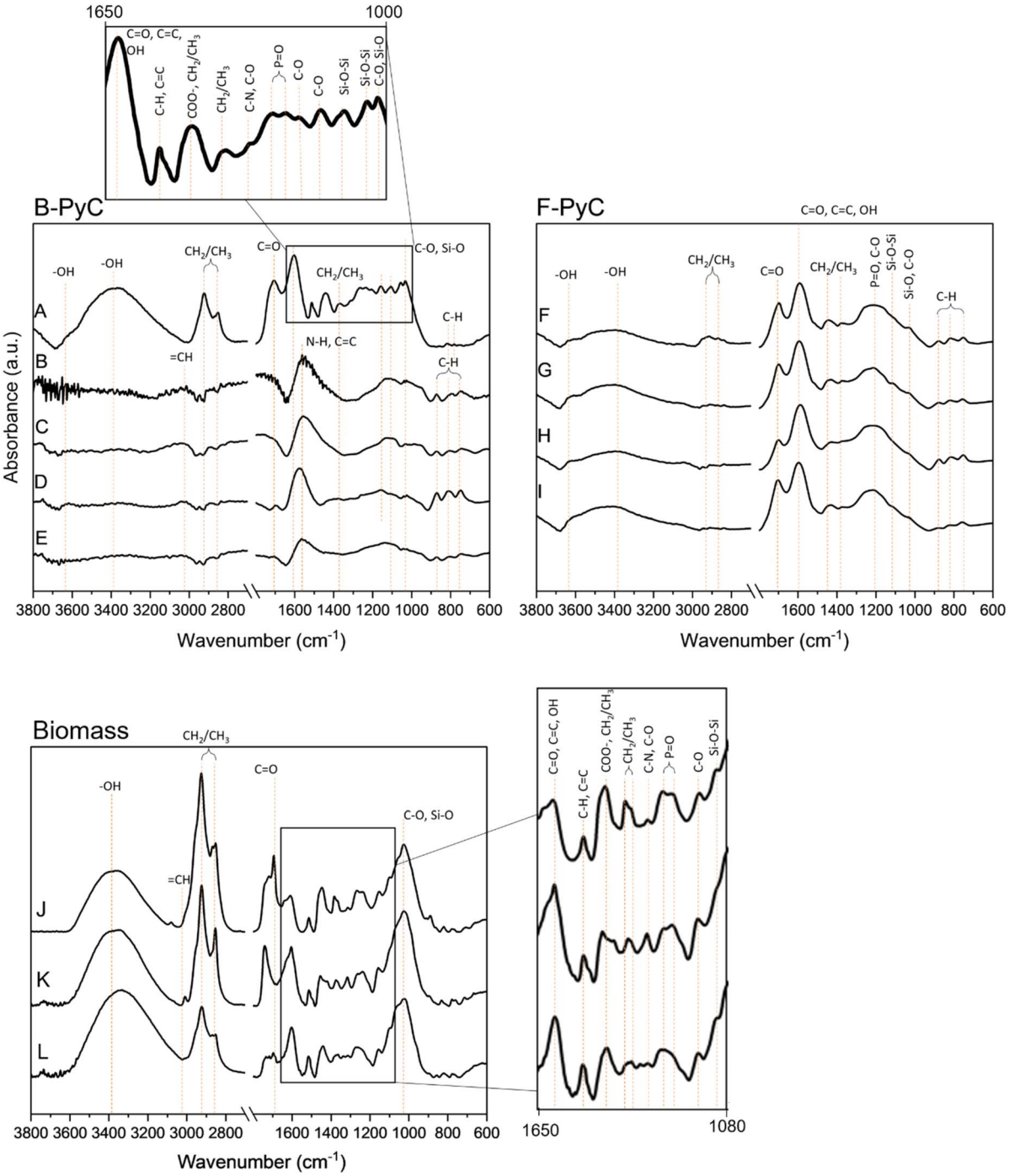

Fig. 3 FT-IR spectra of B-PyC and F-PyC samples: (A) Sp(300/6H/10), (B) Sp(700/6H/10), (C) Pi(700/6H/10), (D) Pi(700/5M/30), (E) Po(700/6H/10), (F) F-PyC(Con), (G) F-PyC(Po), (H) F-PyC(Pi-A), (I) F-PyC(Pi-B), (J) Pi(BM), (K) Po(BM), (L) Sp(BM).[33,38,60,61,65–69] Band assignments with additional interpretation given in Table S8.† Wavenumbers 1800–2700 are omitted due to background noise peaks in this region of the spectra.

includes the C–H stretching of aliphatic CH_2 and CH_3 peaks at 2914 to 2871 cm^{-1}, the characteristic C=O stretch of protonated carboxylic acids at 1710 cm^{-1}, and the –OH stretching at 3645 and 3388 cm^{-1}. Second, the thermal degradation of many C=O and –OH bonds results in a shift of the 1600 cm^{-1} to 1566 cm^{-1}, leaving N–H bending in amides and C=C stretching. Third, we observe the transformation of the dual peaks of C–H out of plane bending in the low-temperature B-PyC (300 °C; 781 and 811 cm^{-1}) to triple peaks in the high-temperature B-PyC (700 °C; 738, 802, and 865 cm^{-1}). These changes appear to be independent of biomass as the absorbance spectra of both Pi(700/6H/10) and Po (700/6H/10) are similar to Sp(700/6H/10). In all the B-PyC samples, there is evidence of the mineral fraction affecting the B-PyC chemistry,

with Si–O stretching peaks of silicates appearing at 1110 cm^{-1} (dual peaks 1105 and 1053 cm^{-1} in Sp(300/6H/10)), and only Sp(300/6H/10) having significant P=O stretching at 1230 and 1240 cm^{-1}. A complete description of band assignments is in Table S8.†

The accelerated pyrolysis of Pi(700/5M/30), when compared with Pi(700/6H/10), results in notable differences (Fig. 3, spectra D and C, respectively). In particular, the aromatic C–H out of plane bending is much more pronounced in Pi(700/5M/30). In addition, there are more preserved structures than in Pi(700/6H/10), specifically C=O and C–O bonds at 1700 and 1176 cm^{-1}, respectively, albeit at a reduced intensity. Additionally, a peak between the low temperature B-PyC peak at 1600 cm^{-1} (C=C, C=O, and –OH stretching of aromatic rings and conjugate ketones) and the higher temperature B-PyC peak at 1566 cm^{-1} (N–H bending of amides) suggests both groups are present. This indicates that accelerating the pyrolysis of Pi(BM) resulted in a potentially more functionalized surface, even at high temperatures (700 °C). This is in contrast to literature that has found the rate of heating and pyrolysis residence time does not significantly impact the surface functionality, with heating rates and residence times during laboratory pyrolysis limited to ≤50 °C min^{-1} and ≥10 min, respectively.[63,64] Our study demonstrates substantial changes in the physicochemical properties of lignin rich B-PyC with an increased pyrolysis rate of as little as 30 °C min^{-1}, and a residence time of 5 min (Fig. 3, spectrum D).

In general, the structural complexity of all F-PyC samples falls between Sp(300/6H/10) and the 700 °C B-PyC samples; Sp(700/6H/10), Pi(700/6H/10), Pi(700/5M/30), and Po(700/6H/10) (Fig. 3, spectra F, G, H, and I). In particular, there is a preservation of –OH bands (3645 and 3388 cm^{-1}), C–H stretching of aliphatic CH_2 and CH_3 groups (2914, 2871, 1463, and 1375 cm^{-1}), C=O stretching of protonated carboxylic acids (1710 cm^{-1}), C=C, C=O, and –OH stretching or aromatic rings (1600 cm^{-1}), and mineral fraction bonds of P=O and Si–O (1230 and 1110 cm^{-1}, respectively). Interestingly, the C–H out of plane bending appears to be in the triple peak form seen in the high-temperature B-PyC, and not double peaks of the lower-temperature B-PyC, Sp(300/6H/10), indicating greater aromatisation and therefore a higher temperature pyrolysis (>300 °C). Collectively, this suggests that the F-PyC material is less pyrolyzed than the high-temperature B-PyC samples, either due to a more rapid pyrolysis or a lower temperature of pyrolysis.[31] As TGA analysis indicates that the temperature of the rapid pyrolysis for F-PyC was greater than the high-temperature B-PyC samples (700 °C), it is likely the former. This is possible due to the very rapid heating rate of wildfires (greater than 50 °C min^{-1}), which is not possible in most pyrolysis units and, additionally, the wildfire time at maximum temperature can be as little as 1 min.[27,28] As the FTIR spectra indicate a less thermally degraded structure, despite the high temperature of pyrolysis, we conclude that rapid pyrolysis during wildfires introduces a kinetics factor to the transformation of organic structures during pyrolysis that is not seen in slower pyrolysis of all B-PyC samples. The FTIR spectra show a kinetics-dependent effect on the chemistry of both B-PyC and F-PyC with the rapid pyrolysis conditions of wildfire activity resulting in a unique functionalized surface. It is also clear that the varied rates and durations of pyrolysis in a wildfire result in differing intensities of functional groups among F-PyC samples, such as carboxyl groups, aromatic compounds, and hydroxyl groups (Fig. 3). These functional groups could translate to differing surface reactivity between F-PyC and slow pyrolysis B-PyC. While not the focus of this study, future work on F-PyC as a possible mechanism of reactive transport should be conducted, given the consistently functionalized surface observed in this study.

3.4 Mobilizable fraction

Mg, Ca, and P had differing leaching behaviours in F-PyC and B-PyC samples due to differing mineralogical compositions (Fig. S11†). Saturation indices confirm the presence of portlandite and that it is the controlling phase on Ca concentrations in slow pyrolysis, high temperature B-PyC (Sp(700/6H/10), Pi(700/6H/10), and Po(700/6H/10)), as found in XRD (Fig. S12 and Table S7†). This differs from low temperature B-PyC, Sp(300/6H/10), and F-PyC, where calcite is the controlling phase. Similarly, brucite ($Mg(OH)_2$) is the controlling phase for slow pyrolysis, high temperature B-PyC and Mg carbonate minerals, such as magnesite or dolomite is the controlling phase for low temperature B-PyC and F-PyC (Fig. S13†). The dissolution of hydroxyapatite ($Ca_5(PO_4)_3OH$) is responsible for leached P concentrations in all samples but slow pyrolysis, high temperature B-PyC (Fig. S12†). A more comprehensive discussion on the mobilizable fraction is available in the ESI.†

The wash treatments demonstrate that the elements B-PyC releases vary not only due to the temperature of pyrolysis (300 °C *versus* 700 °C) but also the duration of pyrolysis (5 min *versus* 6 h). Additionally, the elements released from F-PyC had a composition more similar to the B-PyC produced at a lower maximum temperature and an accelerated rate of pyrolysis (Sp(300/6H/10), Pi(700/5M/10), and Po(700/5M/30) (Fig. S11†). The F-PyC also lacked minerals formed from thermal degradation, such as portlandite and brucite (Fig. S12 and S13†). This indicates that the maximum pyrolysis temperature is not the sole control on the bulk PyC composition, for natural fires (F-PyC) or commercially made (B-PyC). The duration of pyrolysis and the rate of heating also impact the mineralogy and chemical composition of the ash fraction.

It is apparent from characterizing the ash fraction, thermal stability, evolved gases, and mobilizable fraction that F-PyC has properties of both high-temperature fast pyrolysis and low-temperature slow pyrolysis B-PyC. In the absence of mineral phases produced at high temperature, the ash fraction of F-PyC would suggest pyrolysis conditions similar to B-PyC produced at a low temperature. However, the TGA EGA data indicate the opposite, with loss of dehydration and cellulose peaks more similar to the high-temperature, slow pyrolysis B-PyC. This indicates while F-PyC is being produced at similar temperatures to the high-temperature B-PyC studied here (700 °C), the duration of pyrolysis is so short that only the some of the organic

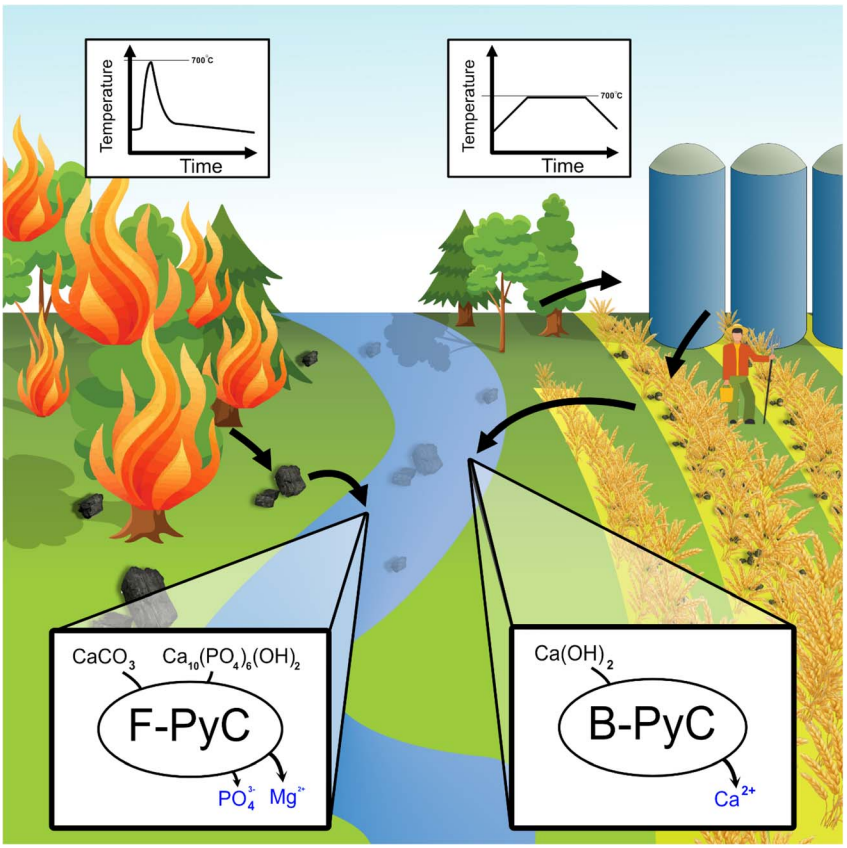

Fig. 4 Schematic diagram illustrating the unique compositional characteristics and resultant elemental leaching of both F-PyC and B-PyC from similar feedstock material and pyrolyzed at approximately the same maximum temperature. Image is not to scale.

fraction is altered to a graphene-like high-temperature product. The inorganic ash fraction undergoes a slower conversion to high-temperature mineralogical products that do not have sufficient time to form in the F-PyC. This suggests that there is an important kinetics component to the thermochemical alteration of components of the organic fraction and the ash fraction of PyC, which have differing rates of conversion. These distinctions also translate to differing leaching potentials and therefore nutrient transport potentials between slow pyrolysis B-PyC and F-PyC.

4. Conclusions

Pyrogenic carbon produced through wildfire activity, F-PyC, is an influential and predominant component of the carbon cycle.[1,29] While the physicochemical properties of commercially produced B-PyC have been extensively explored in the literature due to its application in remediation and soil amendment, F-PyC has not been studied as thoroughly. In this regard, our work represents one of the first attempts to investigate the chemical composition of F-PyC and B-PyC made from the same biomass.[16–21,24] Our findings demonstrate that during forest fires the accelerated pyrolysis at high temperatures, occurring under variable atmospheric oxygen, and then rapid cooling produces PyC that is distinct from B-PyC in multiple aspects. TGA analyses indicating that the F-PyC being produced at high temperatures, more similar to that of the high temperature B-PyC (700 °C) than the low temperature B-PyC (300 °C). Despite this, the F-PyC samples are characterized by: (1) an elemental composition reminiscent of B-PyC produced at lower temperatures (<700 °C); (2) an ash fraction consisting of minerals stable under lower temperatures, leading to differing elemental leaching; and (3) a chemical surface featuring bonded molecules similar to B-PyC generated at lower temperatures (>300 °C but <700 °C). These differences stem primarily from the unique heating and cooling rates, as well as pyrolysis durations, associated with F-PyC, which introduce a kinetics factor to the thermochemical alteration of biomass. This kinetics factor results in inherent compositional differences between F-PyC and conventional B-PyC, suggesting that much of the physicochemical data on B-PyC is likely not applicable to F-PyC (Fig. 4). Thus, our study finds further support from the findings of Santín *et al.* (2017) that in terms of the physicochemical properties, slow-pyrolysis B-PyC is not a suitable proxy for F-PyC.[26]

These different physicochemical properties result in markedly different interactions in natural environments. For example, B-PyC is often used as a soil amendment due to its slow release of nutrient elements.[16,22,70] In contrast, the mineralogical composition of the ash fraction of F-PyC is composed of minerals stable at lower temperatures, some of which require more extended weathering periods to dissolve in natural

systems, such as calcite, which would result in an even slower release of many nutrient elements than a comparable B-PyC. Therefore, F-PyC may possess a greater long-term capacity to fertilize soil compared to B-PyC derived from the same biomass. The release of other elements should also be considered, as F-PyC leaches many elements which may affect water quality in riverine systems.[71–73] This study highlights the unique physicochemical properties of F-PyC, which result from the rapid pyrolysis conditions found in wildfires. Future work should further investigate these differences by exploring how they influence the surface reactivity and nutrient and metals adsorption potential of F-PyC. This information could be used to determine the importance of F-PyC in elemental transport models as compared to other known transport mechanisms, such as clays and bacteria. Additionally, future field work should be conducted to understand how F-PyC properties vary with rapidly changing and ephemeral wildfire burn temperatures and conditions, using thermocouple measurements as well as collecting gas composition measurements at points of pyrolysis during controlled burns.

Data availability

The data supporting this article have been included as part of the ESI.†

Author contributions

The manuscript was written through contributions of all authors. All authors have given approval to the final version of the manuscript.

Conflicts of interest

There are no conflicts of interest to declare.

Acknowledgements

The work conducted in this study was supported by Natural Sciences and Engineering Research Council of Canada (NSERC) Discovery Grants to D. S. A. (RGPIN-2020-05289), K. O. K. (RGPIN-2020-05189), and J. P. L. K. (RGPIN-2021-02787) as well as a NSERC CGS-D Scholarship to K. N. S. The authors would like to thank the British Columbia Wildfire Service, particularly Fons Raedschelders of the Southeast Fire Center for providing information about the fire as well as contacts to safely conduct sampling. Additionally, the support provided by Louisiana-Pacifica Building Solutions, particularly Tim Arnett and Peter Russell for accommodating us during their logging season and allowing access during operations to collect samples. Finally, the authors thank Cijo Xavier at Newcastle University for conducting TGA analyses.

References

1 C. Santín, S. H. Doerr, E. S. Kane, C. A. Masiello, M. Ohlson, J. M. de la Rosa, C. M. Preston and T. Dittmar, Towards a global assessment of pyrogenic carbon from vegetation fires, *Glob. Change Biol.*, 2016, **22**, 76–91.

2 M. W. Jones, C. Santín, G. van der Werf and S. H. Doerr, Global fire emissions buffered by the production of pyrogenic carbon, *Nat. Geosci.*, 2019, **12**, 742–747.

3 B. Zheng, P. Ciasis, F. Chevallier, E. Chuvieco, Y. Chen and H. Yang, Increasing forest fire emissions despire the decline in global burn area, *Sci. Adv.*, 2021, **7**(39), 1–8.

4 B. Zheng, P. Ciasis, F. Chevallier, H. Yang, J. G. Canadell, Y. Chen, I. R. van der Velde, I. Aben, E. Chuvieco and Q. Zhang, Record-high CO_2 emissions from boreal fires in 2021, *Science*, 2023, **379**(6635), 1–6.

5 A. I. Coppola, D. B. Wiedemeier, V. Galy, N. Haghipour, U. M. Hanke, G. S. Nascimento, M. Usman, T. M. Blattmann, M. Reisser, C. V. Freymond, M. Zhao, B. Voss, L. Wacker, E. Schefus, B. Peucker-Ehrenbrink, S. Abiven, M. W. I. Schmidt and T. I. Eglinton, Global-scale evidence for refractory nature of riverine black carbon, *Nat. Geosci.*, 2018, **11**, 584–588.

6 J. E. Halofsky, D. L. Peterson and B. J. Harvey, Changing wildfire, changing forests: the effects of climate change on fire regimes and vegetation in the Pacific Northwest, USA, *Fire Ecol.*, 2020, **16**(4), 1–26.

7 M. Turco, J. T. Abatzoglou, S. Herrera, Y. Zhuang, S. Jerez, D. D. Lucas, A. AghaKouchak and I. Cvijanovic, Anthropogenic climate change impacts exacerbate summer forest fires in California, *Proc. Natl. Acad. Sci. USA*, 2023, **120**(25), 1–9.

8 C. C. Hanes, X. Wang, P. Jain, M. A. Parisien, J. M. Little and M. D. Flannigan, Fire-regime changes in Canada over the last half century, *Can. J. For. Res.*, 2019, **49**, 256–269.

9 E. S. Kasischke and M. R. Turetsky, Recent changes in the fire regime across the North American boreal region–Spacial and temporal patterns of burning across Canada and Alaska, *Geophys. Res. Lett.*, 2006, **33**(9), 1–5.

10 M. A. Parisien, Q. E. Barber, M. L. Bourbonnais, L. D. Daniels, M. D. Flannigan, R. W. Gray, K. M. Koffman, P. Jain, S. L. Stephens, S. W. Taylor and E. Whitman, Abrupt, climate-induced increase in wildfires in British Columbia since the mid-2000s, *Commun. Earth Environ.*, 2023, **4**(309), 1–11.

11 C. A. Phillips, B. M. Rogers, M. Elder, S. Cooperdock, M. Moubarak, J. T. Randerson and P. C. Frumhoff, Escalating carbon emissions from North American boreal foret wildfires and the climate mitigation potential of fire management, *Sci. Adv.*, 2022, **8**(17), 1–9.

12 M. Senande-Rivera, D. Insua-Costa and G. Miguez-Macho, Spatial and temporal expansion of global wildland fire activity in response to climate change, *Nat. Commun.*, 2022, **13**(1208), 1–9.

13 IBI, Standardized product definition and product testing guidelines for biochar that is used in soil, *International Biochar Initiative*, 2012, 2015.

14 J. Lehmann, A. Cowle, C. A. Masiello, C. Kammann, D. Woolf, J. E. Amonette, M. L. Cayuela, M. Camps-Arbestain and T. Whitman, Biochar in climate change mitigation, *Nat. Geosci.*, 2021, **14**, 883–892.

15 A. I. Coppola, S. Wagner, S. T. Lennartz, M. Seidel, N. Ward, T. Dittmar, C. Santín and M. W. Jones, The black carbon cycle and its role in the Earth system, *Nat. Rev. Earth Environ.*, 2022, **3**, 516–532.
16 K. von Gunten, M. S. Alam, M. Hubmann, Y. S. Ok, K. O. Konhauser and D. S. Alessi, Modified sequential extraction for biochar and petroleum coke: Metal Release potential and its environmental implications, *Bioresour. Technol.*, 2017, **236**, 106–110.
17 M. S. Alam, D. Gorman-Lewis, N. Chen, S. L. Flynn, Y. S. Ok, K. O. Konahuser and D. S. Alessi, Thermodynamic Analysis of Nickel(II) and Zinc (II) Adsorption to Biochar, *Environ. Sci. Technol.*, 2018, **52**(11), 6246–6255.
18 M. S. Alam, D. Gorman-Lewis, N. Chen, S. Safari, K. Baek, K. O. Konhauser and D. S. Alessi, Mechanisms of the removal of U(VI) from aqueous solution using biochar: A combined spectroscopic and modeling approach, *Environ. Sci. Technol.*, 2018, **52**(22), 13057–13067.
19 M. S. Alam and D. S. Alessi, Modeling the surface chemistry of biochars. in, *Biochar from Biomass and Waste*, Ok, Y. S., Tsang, D. C. W., Bolan, N. and Novak, J. M., ed. Elsevier, 1st edn, Amsterdam, Netherlands, (2019), pp. 59–72.
20 H. Gong, Z. Tan, L. Zhang and Q. Huang, Preparation of biochar with high absorbability and its nutrient adsorption-desorption behaviour, *Sci. Total Environ.*, 2019, **694**, 133728.
21 T. G. Ambaye, M. Vaccari, E. D. van Hullebusch and A. S. Rtimi, Mechanisms and adsorption capacities of biochar for the removal of organic and inorganic pollutants from industrial wastewater, *Int. J. Environ. Sci. Technol.*, 2021, **18**, 3273–3294.
22 M. Ahmad, A. U. Rajapaksha, J. E. Lim, M. Zhang, N. Bolan, D. Mohan, M. Vithanage, S. S. Lee and Y. S. Ok, Biochar as a sorbent for contaminant management in soil and water: a review, *Chemosphere*, 2014, **99**, 19–33.
23 Y. Ding, Y. Liu, S. Liu, Z. Li, X. Tan, X. Huang, G. Zeng, L. Zhou and B. Zheng, Biochar to improve soil fertility, *Agron. Sustain. Dev.*, 2016, **36**, 1–18.
24 H. Zheng, Z. Wang, X. Deng, J. Zhao, Y. Luo, J. Novak, S. Herbert and B. Xing, Characteristics and nutrient values of biochars produced from giant reed at different temperatures, *Bioresour. Technol.*, 2013, **130**, 463–471.
25 Z. Ye, L. Liu, Z. Tan, L. Zhang and Q. Huang, Effects of pyrolysis conditions on migration and distribution of biochar nitrogen in the soil-plant-atmosphere system, *Sci. Total Environ.*, 2020, **25**, 138006.
26 C. Santín, S. H. Doerr, A. Merino, T. D. Bucheli, R. Bryant, P. Ascough, X. Gao and C. A. Masiello, Carbon sequestration potential and physicochemical properties differ between wildfire charcoals and slow-pyrolysis biochars, *Sci. Rep.*, 2017, **7**, 11233.
27 A. C. Scott, D. M. J. S. Bowman, W. J. Bond, S. J. Pyne, and M. E. Alexander, *Earth on Fire: an Introduction*, Wiley-Blackwell, (2014), pp. 434.
28 C. Santín, S. H. Doerr, A. Merino, R. Bryant and N. J. Loader, Forest floor chemical transformations in a boreal forest fire and their correlations with temperature and heating duration, *Geoderma*, 2016, **264**, 71–80.
29 L. J. Tranvik, New light on black carbon, *Nat. Geosci.*, 2018, **11**, 547–548.
30 C. M. Belcher and V. A. Hudspith, The formation of charcoal reflectance and its potential use in post-fire assessments, *Int. J. Wildland Fire*, 2016, **25**, 775–779.
31 J. M. Cerrato, J. M. Blank, C. Hirani, A. L. Clark, A. S. Ali, K. Artyushkova, E. Petersonm and R. J. Bixby, Wildfires and water chemistry: effect of metals associated with wod ash, *Environ. Sci.: Processes Impacts*, 2016, **18**, 1078–1089.
32 B. Glaser and J. J. Birk, State of the scientific knowledge on properties and genesis of Anthropogenic Dark Earths in Central Amazonia (*terra preta de Índio*), *Geochim. Cosmochim. Acta*, 2012, **82**, 39–51.
33 T. Sun, B. D. A. Levin, J. J. L. Guzman, A. Enders, D. A. Muller, L. T. Angenent and J. Lehmann, Rapid electron transfer by the carbon matrix in natural pyrogenic carbon, *Nat. Commun.*, 2017, **8**, 14873.
34 A. Howell, S. Helmkamp and E. Belmont, Stable polycyclic aromatic carbon (SPAC) formation in wildfire chars and engineered biochars, *Sci. Total Environ.*, 2022, **849**, 157610.
35 E. Srebotnik and K. Messner, A simple method that uses differential staining and light microscopy to assess the selectivity of wood delignification by white rot fungi, *Appl. Environ. Microbiol.*, 1994, **4**, 1383–1386.
36 Richter, H. G., Grosser, D., Heinz, I. and Gasson, P. E., (ed), *IAWA list of microscopic features for softwood identification*, IAWA Journal, (2004), vol. 25, (1), pp. 1–70.
37 Wheeler, E. A., Baas, P. and Gasson, P. E., (ed), *IAWA list of microscopic features for hardwood identification*, IAWA Bulletin, (1989), vol. 10, (3), pp. 219–332.
38 K. K. Pandey, A study of Chemical Structure of Softwood and Hardwood and Wood Polymers by FTIR Spectroscopy, *J. Appl. Polym. Sci.*, 1999, **71**(12), 1969–1975.
39 Ministry of Forests, Trembling Aspen. Province of British Columbia. Retrieved from, **https://www2.gov.bc.ca/gov/content/industry/forestry/managing-our-forest-resources/silviculture/tree-species-selection/tree-species-compendium-index/trembling-aspen**, 2023.
40 Ministry of Forests, Lodgepole Pine. Province of British Columbia. Retrieved from, **https://www2.gov.bc.ca/gov/content/industry/forestry/managing-our-forest-resources/silviculture/tree-species-selection/tree-species-compendium-index/lodgepole-pine**, 2023.
41 Ministry of Forests Engelmann Spruce. Province of British Columbia. Retrieved from **https://www2.gov.bc.ca/gov/content/industry/forestry/managing-our-forest-resources/silviculture/tree-species-selection/tree-species-compendium-index/engelmann-spruce**, 2023.
42 A. Enders and J. Lehmann, Comparison of Wet-Digestion and Dery-Ashing Methods for Total Elemental Analysis of Biochar, *Commun. Soil Sci. Plant Anal.*, 2012, **43**(7), 1042–1052.
43 M. Neumann, R. Nöske, G. Bach, T. Glaubauf, M. Bartoszek and P. Strauch, A Procedure for Rapid Determination of the Silicon Content in Plant Materials, *Z. Naturforsch.*, 2011,

66(3), 289–294; M. N. Nguyen, Potential use of silica-rich biochar for the formulation of adaptively controlled release fertilizers: A mini review, *J. Clean. Prod.*, 2021, **307**, 127188.

44 D. Parkhurst and C. A. J. Appelo, PHREEQC (Version 4)–A Computer Program for Speciation, Batch Reaction, One-Dimensional Transport, and Inverse Geochemical Calculations, *US Geologic Survey, Water Resources Divisions*, Denver, Co, (2013).

45 K. N. Snihur, L. R. Swaren, K. von Gunten, N. B. Harris, S. Wilson, M. K. Gingras, K. O. Konhauser, S. L. Flynn and D. S. Alessi, Effects of salinity on the leaching of ionic species from hydrocarbon target formations during hydraulic fracturing, *Chem. Geol.*, 2022, **591**, 120718.

46 J. Felten, H. Hall, J. Jaumot, R. Tauler, A. D. Juan and A. Gorzsás, Vibrational spectroscopic image analysis of biological material using multivariate curve resolution-alternating least squares (MCR-ALS), *Nat. Protoc.*, 2015, **10**, 217–240.

47 I. Naydenova, T. Radoykova, T. Petrova, O. Sandov and I. Valchev, Utilization Perspectives of Lignin Biochar from Industrial Biomass Residue, *Molecules*, 2023, **28**, 4842.

48 L. Gašparovič, Z. Koreňová and L. Jelemenský, Kinetic study of wood chips decomposition by TGA, *Chem. Pap.*, 2010, **64**(2), 174–181.

49 M. Brebu and C. Vasile, Thermal degradation of lignin–a review, *Cellul. Chem. Technol.*, 2010, **44**(9), 353–363.

50 S. Gezahegn, M. Sain and S. C. Thomas, Phytotoxic condensed organic compounds are common in fast but not slow pyrolysis biochar, *Bioresour. Technol. Rep.*, 2021, **13**, 10061351.

51 E. W. Bruun, P. Ambus, H. Egsgaard and H. Hauggaard-Nielsen, Effects of slow and fast pyrolysis biochar on soil C and N turnover dynamics, *Soil Biol. Biochem.*, 2012, **46**, 73–79.

52 H. Tan, C. T. Lee, P. Y. Ong, K. Y. Wong, C. P. C. Bong, C. Li and Y. Gao, A Review On The Comparison Between Slow Pyrolysis And Fast Pyrolysis On the Quality Of Lignocellulosic And Lignin-Based Biochar. IOP Conf. Ser, *Mater. Sci. Eng.*, 2021, **1051**, 012075.

53 X. Zhu, Y. Li and X. Wang, Machine learning prediction of biochar yield and carbon content based on biomass characteristics and pyrolysis conditions, *Bioresour. Technol.*, 2019, **288**, 121527.

54 A. Lataf, M. Jozefczak, B. Vandecasteele, J. Viaene, S. Schreurs, R. Carleer, J. Yperman, W. Maerchal, A. Cuypers and D. Vandamme, The effect of pyrolysis temperature and feedstock on biochar agronomic properties, *J. Anal. Appl. Pyrolysis*, 2022, **168**, 105728.

55 S. Zhao, N. Ta and X. Wang, Effect of Temperature on the Structural and Physicochemical Properties of Biochar with Apple Tree Branches as Feedstock Material, *Energies*, 2017, **10**(9), 1293.

56 T. A. Coates, A. T. Chow, D. L. Hagan, T. A. Waldrop, G. G. Wang, W. C. Bridges, M. Rogers and J. H. Dozier, Thermocouple Probe Orientation Affects Prescribed Fire Behaviour Estimation, *J. Environ. Qual.*, 2018, **47**(1), 170–176.

57 B. M. Wotton, J. S. Gould, W. L. McCas, N. P. Cheney and S. W. Taylor, Flame temperature and residence time of fires in dry eucalypt forest, *Int. J. Wildland Fire*, 2012, **21**, 270–281.

58 C. Sánchez-García, C. Santín, J. Neris, G. Sigmund, X. L. Otero, J. Manley, G. González-Rodríguez, C. M. Belcher, A. Cerdà, A. L. Marcotte, S. F. Murphy, C. C. Rhoades, G. Sheridan, T. Strydom, P. R. Robichaud and S. H. Doerr, Chemical characteristics of wildfire ash across the globe and their environmental and socio-economic implications, *Environ. Int.*, 2023, **178**, 108065.

59 Z. Dai, Y. Wang, N. Muhammad, K. Xiao, J. Meng, X. Liu, J. Xu and P. C. Brookes, The effects and mechanisms of soil acidity changes, following incorporation of biochars in three soils differing in initial pH, *Soil Sci. Soc. Am. J.*, 2014, **78**(5), 1606–1614.

60 Z. Chen, X. Xiao, B. Chen and L. Zhu, Quantification of Chemical States, Dissociation Constants and Contents of Oxygen-containing Groups on the Surface of Biochar Produced at Different Temperatures, *Environ. Sci. Technol.*, 2015, **49**, 309–317.

61 R. Janu, V. Mrlik, D. Ribitsch, J. Hofman, P. Sedláček, L. Bielská and G. Soja, Biochar surface functional groups as affected by biomass feedstock, biochar composition and pyrolysis temperature, *Carbon Resour. Convers.*, 2021, **4**, 36–46.

62 M. Keiluweit, P. S. Nico, M. G. Johnson and M. Kleber, Dynamic Molecular Structure of Plant Biomass-Derived Black Carbon (Biochar), *Environ. Sci. Technol.*, 2010, **44**, 1247–1253.

63 D. Angin, Effect of pyrolysis temperature and heating rate on biochar obtained from pyrolysis of safflower seed press cake, *Bioresour. Technol.*, 2013, **128**, 593–597.

64 B. Zhao, D. O/Conner, J. Zhang, T. Peng, Z. Shen, D. C. W. Tsang and D. Hou, Effect of pyrolysis temperature, heating rate, and residence time on rapeseed stem derived biochar, *J. Clean. Prod.*, 2018, **174**, 977–987.

65 R. Ellerbrock, M. Stein and J. Schaller, Comparing amorphous silica, short-range-ordered silicates and silicic acid species by FTIR, *Sci. Rep.*, 2022, **12**, 11708.

66 J. P. L. Kenney and A. Gorzsas, Applications of fourier-transform infrared spectroscopy in geomicrobiology, "*Analytical Geomicrobiology: a Handbook of Instrumental Techniques*", (2019), pp. 288–313.

67 S. J. Parikh and J. Chorover, ATR-FTIR study of lipopolysaccharides at mineral surfaces, *Colloids Surf., B*, 2008, **62**(2), 188–198.

68 G. Soctrates, *Infrared and Raman Characteristic Group Frequencies*, John Wiley and Sons, (3rd edn), New York, (2001).

69 V. Ţucureanu, A. Matei and A. M. Avram, FTIR Spectroscopy for Carbon Family Study, *Crit. Rev. Anal. Chem.*, 2016, **46**, 502–520.

70 C. Wang, D. Lou, X. Zhang, R. Huang, Y. Cao, G. Liu, Y. Zhang and H. Wang, Biochar-based slow-release

fertilizer for sustainable agriculture: a mini review, *Environ. Sci. Ecotechnology*, 2022, **10**, 100167.
71 M. T. Beyene, S. G. Liebowitz, C. J. Dunn and K. D. Bladon, To burn or not to burn: An empirical assessment of the impacts of wildfires and prescribed fires on trace element concentrations in Western US streams, *Sci. Total Environ.*, 2023, **863**, 160731.
72 K. D. Bladon, M. B. Emelko, U. Silins and M. Stone, Wildfire and the Future of Water Supply, *Environ. Sci. Technol.*, 2014, **48**, 8936–8943.
73 M. J. Paul, S. D. LeDuc, M. G. Lassiter, L. C. Moorhead, P. D. Noyes and S. G. Leibowitz, Wildfire induces changes in receiving waters: a review with considerations for water quality management, *Water Resour. Res.*, 2022, **58**(9), 1–28.